



HAL
open science

Proton Equatorial Pitch Angle Distributions in Jupiter's Inner Magnetosphere

Y. Sarkango, J R Szalay, A R Poppe, Q. Nénon, P. Kollmann, G. Clark, D J Mccomas

► **To cite this version:**

Y. Sarkango, J R Szalay, A R Poppe, Q. Nénon, P. Kollmann, et al.. Proton Equatorial Pitch Angle Distributions in Jupiter's Inner Magnetosphere. *Geophysical Research Letters*, 2023, 50 (11), pp.e2023GL104374. 10.1029/2023GL104374 . hal-04299669

HAL Id: hal-04299669

<https://hal.science/hal-04299669>

Submitted on 22 Nov 2023

HAL is a multi-disciplinary open access archive for the deposit and dissemination of scientific research documents, whether they are published or not. The documents may come from teaching and research institutions in France or abroad, or from public or private research centers.

L'archive ouverte pluridisciplinaire **HAL**, est destinée au dépôt et à la diffusion de documents scientifiques de niveau recherche, publiés ou non, émanant des établissements d'enseignement et de recherche français ou étrangers, des laboratoires publics ou privés.

Geophysical Research Letters[®]



RESEARCH LETTER

10.1029/2023GL104374

Key Points:

- 10–50 keV protons at Jupiter are predominantly field-aligned at M-shells between $M = 7$ and $M = 20$
- Normalized pitch angle distributions of >200 keV protons show evidence of adiabatic acceleration during inward radial transport
- Observed proton distributions could result from charge-exchange with neutrals or conservation of adiabatic invariants during transport

Supporting Information:

Supporting Information may be found in the online version of this article.

Correspondence to:

Y. Sarkango,
sarkango@princeton.edu

Citation:

Sarkango, Y., Szalay, J. R., Poppe, A. R., Nénon, Q., Kollmann, P., Clark, G., & McComas, D. J. (2023). Proton equatorial pitch angle distributions in Jupiter's inner magnetosphere. *Geophysical Research Letters*, 50, e2023GL104374. <https://doi.org/10.1029/2023GL104374>





Received 1 MAY 2023

Accepted 1 JUN 2023

© 2023 The Authors.

This is an open access article under the terms of the [Creative Commons Attribution-NonCommercial License](#), which permits use, distribution and reproduction in any medium, provided the original work is properly cited and is not used for commercial purposes.

Proton Equatorial Pitch Angle Distributions in Jupiter's Inner Magnetosphere

Y. Sarkango¹ , J. R. Szalay¹ , A. R. Poppe² , Q. Nénon³ , P. Kollmann⁴ , G. Clark⁴ , and D. J. McComas¹ 

¹Department of Astrophysical Sciences, Princeton University, Princeton, NJ, USA, ²Space Sciences Laboratory, University of California, Berkeley, CA, USA, ³IRAP: Institut de Recherche en Astrophysique et Planetologie, CNRS-UPS-CNRS Toulouse, Toulouse, France, ⁴The Johns Hopkins University Applied Physics Laboratory, Laurel, MD, USA

Abstract We use data from the plasma and energetic particle instruments on the *Juno* spacecraft, JADE and JEDI, to study the equatorial pitch angle distributions of energetic protons within Jupiter's inner magnetosphere during *Juno*'s prime mission from 2016 to 2021. Averaging over all observations made by *Juno* within M-shell bins between $M = 6$ and $M = 30$, we find protons at energies between 10 and 50 keV are predominantly field-aligned at all M-shells. In contrast, those at energies above 200 keV transition from being predominantly field-aligned at $M = 20$ to having pancake-like distributions at $M < 10$. We find the observed distributions are consistent either with charge exchange of protons with neutral toroidal clouds, or with adiabatic acceleration of protons originating from Jupiter that are transported inward from the middle magnetosphere.

Plain Language Summary Protons are seen throughout Jupiter's magnetosphere. Where these protons come from and how they evolve is not well understood. Previous observations by the *Galileo* spacecraft showed that protons in the vicinity of Europa have properties consistent with charge exchange with a neutral species, which effectively removes the charged particles from the magnetosphere. Using data from the *Juno* spacecraft, we survey proton distributions at different energies. Although charge exchange remains a plausible explanation for the observations, another possibility is that the distribution is a result of adiabatically transporting the protons through Jupiter's magnetic field.

1. Introduction

Jupiter's inner magnetosphere plasma is primarily comprised of heavy ions in the form of O^{n+} or S^{n+} and protons (H^+) (Bagenal et al., 2016; Bodisch et al., 2017; Bridge et al., 1979; Dougherty et al., 2017; Frank et al., 1996; Kim et al., 2020; Kollmann et al., 2018). While the heavy ions are believed to be products of ionization of neutrals from Io, the protons may have several possible sources (Jupiter, its moons or the solar wind) that have not been well constrained (e.g., Bodisch et al., 2017; Hamilton et al., 1980; Szalay et al., 2021).

Protons have been observed in the equatorial Jovian magnetosphere over a wide range of energies from a few eV to several tens of MeV. Kollmann et al. (2017) combined data from the *Pioneer 11*, *Galileo* and *Juno* spacecraft to show that proton fluxes in the keV-to-MeV range are highest in the inner magnetosphere but decrease sharply inward of Io's orbit. Shen et al. (2022) used data from *Juno*'s energetic particle detector (JEDI) and found an increase in 453–542 keV and 0.9–2 MeV proton flux while moving inward. The pitch angle distributions at these energies transitioned from nearly field-aligned at $30 R_J$ ($1 R_J = 71,492$ km) to pancake-like with a maximum flux at 90° near $10 R_J$. However, the same behavior was not observed for protons with energies between 106 and 122 keV. A similar pitch angle transition from field-aligned or butterfly to pancake-like was reported by Tomás et al. (2004) for 80–220 keV protons and, 29–42 keV and 304–527 keV electrons.

Lagg et al. (2003) observed that at energies between 80 and 220 keV, proton distributions in the vicinity of Europa had minimum flux at 0° and 90° pitch angle, whereas protons between 220–540 keV and 0.54–1 MeV had pancake-like pitch angle distributions. The butterfly-like distributions (with minimum flux at 90°) observed for the 80–220 keV population were similar to those of heavy ions observed near the orbit of Io (Lagg et al., 1998). Charge exchange with neutral atoms or cold ions could deplete near-perpendicular fluxes as these ions would spend more time in the high neutral density equatorial regions over the course of their bounce motion (Clark et al., 2016; Ip, 1981; Kollmann et al., 2016; Lagg et al., 2003; Mauk et al., 2004; Nénon & André, 2019). Hence, butterfly pitch angle distributions occurring only at lower energies below a few hundred keV was also consistent

with typical ion-neutral charge exchange cross-sections decreasing with increasing energy above ~ 10 keV (Lindsay & Stebbings, 2005).

Assuming ion-neutral charge exchange was responsible for the observed proton flux depletions, the observations were suggested to be consistent with a Europa neutral torus of O with density between 20 and 40 cm^{-3} (Lagg et al., 2003). These inferred neutral densities were also commensurate with ENA observations by Mauk et al. (2003) and with models of neutral escape from the moons (Smith et al., 2019; Smyth & Marconi, 2003, 2006), but not with the lack of atomic oxygen emissions reported by Hansen et al. (2005) and Shemansky et al. (2014). Moreover, numerical simulations have predicted that H_2 , not O, is the most abundant neutral species at the orbit of Europa with a nominal H_2 density of $\sim 30 \text{ cm}^{-3}$ in the Europa neutral torus, although this could increase up to $\sim 200 \text{ cm}^{-3}$ in the vicinity of Europa. In the Smith et al. (2019) model, the Europa-genic H_2 and O tori were quite broad and occupied a region from ~ 5 to $\sim 15 R_J$. Observations from *Juno* of H_2^+ pickup-ions from a Europa-genic source provided evidence of a persistent neutral source of H_2 of between 0.5 and 1.9 kg s^{-1} in the vicinity of Europa's orbit (Szalay, Smith, et al., 2022).

Kollmann et al. (2016) showed that proton fluxes near Europa were lowest at around 70° equatorial pitch angle rather than 90° . This could be explained by ions undergoing charge exchange with a thinner neutral torus that is confined to smaller latitudes about the Jovigraphic equator. Kollmann et al. (2016) assumed that the neutral torus mainly consisted of H_2 and found that the observations required an H_2 density in the range of 1.5–410 cm^{-3} , depending on assumed transport rates. In addition, Nénon and André (2019) found that the sulfur ion fluxes were depleted near 90° pitch angle for some of *Galileo*'s orbits near Europa. They hypothesized that the different distributions for protons and sulfur ions could be explained by the presence of neutral tori of O and H_2 with different scale heights.

While the observed proton distributions appear consistent with charge exchange related losses, it is also important to consider other processes that could create similar distributions. Unlike heavy ions ($\text{O}^{n+}/\text{S}^{n+}$), which come from the equatorial magnetosphere mainly as pickup-ions through electron-impact ionization, proton sources in Jupiter's magnetosphere are less well understood (Bagenal & Dols, 2020). *Juno* observed up-welling proton beams contributing 1–5 kg/s of proton outflow from the polar regions of Jupiter (Szalay et al., 2021) along with conic distributions connected to Io's orbit (Clark et al., 2020) and between 3 and 5 R_J in the polar-most regions (Szalay, Clark, et al., 2022). These suggest wave-particle interactions can also lead to protons being injected into the magnetosphere from Jupiter. In the absence of wave-particle scattering, H^+ ions originating from the polar regions of Jupiter are expected to be highly field-aligned when they reach the equatorial magnetosphere due to the ratio of the polar to equatorial magnetic field strength and the conservation of the first adiabatic invariant (similar to electron observations by Frank & Paterson, 2002). Hence, the proton butterfly pitch angle distributions observed by *Galileo* could also result from adiabatic transport from Jupiter's polar regions instead of charge exchange with neutrals.

In this work, we survey the equatorial pitch angle distributions of protons in the inner magnetosphere of Jupiter. We combine data from *Juno*'s JADE and JEDI particle detectors to examine distributions of protons with energies between 10 and 700 keV. Our work extends previous work from Shen et al. (2022) by including the <50 keV proton population between 6 and 20 R_J in terms of equatorial pitch angle. In Section 2, we describe the methodology we use to analyze and combine multiple charged particle datasets from *Juno*. In Section 3, we describe the observations in the region past Io to Ganymede. Using the pitch angle distributions, we discuss implications for ion-neutral charge exchange and proton transport in the magnetosphere. We conclude in Section 4 with a summary of our results and address the question of whether proton distributions observed previously were consistent with charge exchange with a neutral torus.

2. Methodology

We analyze data collected by the plasma and energetic particle instruments onboard the *Juno* spacecraft during its prime mission. The JADE-I instrument (McComas et al., 2017) measures lower energy plasma and energetic ions between 10 eV/q to 50 keV/q. The JEDI instrument (Mauk, Haggerty, Jaskulek, et al., 2017; Mauk et al., 2023) measures higher energy ions, including protons between 40 keV and 20 MeV.

JADE-I has a field-of-view that covers the full sky for each *Juno* spin period of ~ 30 s and therefore has complete pitch angle coverage on a cadence of 30 s. However, extracting the pitch angle distribution in the plasma rest

frame requires prior knowledge of the plasma flow velocity with respect to the spacecraft, which is non-trivial (see Appendix in Szalay et al., 2020). Without knowing the plasma speed, pitch angle alone does not organize the directional distribution well and another coordinate such as a clock angle around the field direction would be needed. For this reason, we limit the analysis of JADE pitch angle distributions to protons above 10 keV since ion velocities at these relatively high energies much larger than the bulk flow velocity.

Higher energy ion fluxes >50 keV are measured by the JEDI-90 and JEDI-270 sensors, and both have a field-of-view that is $160^\circ \times 12^\circ$ with the wide azimuthal portion nearly aligned with the *Juno* spin plane. Hence, the JEDI sensors measure the full pitch angle distribution (PAD) only when the background magnetic field is within $\pm 6^\circ$ of the *Juno* spin plane, otherwise there are gaps in the distribution. We group the JEDI proton fluxes into two energy ranges: (a) 50–200 keV, where the bulk of charge-exchange is expected (Lindsay & Stebbings, 2005), and (b) 200–700 keV. We chose these energy ranges as charge-exchange cross-sections decrease sharply above ~ 100 keV for both H^+ -O and H^+ -H₂ reactions (see Supporting Information S1) and the lifetime for an energetic particle to charge exchange with a neutral atom is inversely proportional to its velocity (Lagg et al., 1998). JEDI proton channels below 50 keV are ignored to avoid data that is contaminated by penetrating electrons and electronic noise (Mauk, Haggerty, Paranicas, et al., 2017). The data from both JADE and JEDI instruments are averaged to 5-min cadence for analysis.

We constructed proton equatorial pitch angle distributions between M-shells $M = 5$ and $M = 30$. An M-shell is defined by the maximum radial extent of the magnetic field line. We use M-shell instead of L-shell to differentiate between the dipolar field at Earth versus Jupiter where the non-dipolar field contributions from the internal magnetic field and current sheet are significant. The local pitch-angle is calculated by using the magnetic field measured by *Juno*'s magnetometer (Connerney et al., 2017). The equatorial pitch angle α_{eq} is related to the local pitch angle α as,

$$\alpha_{eq} = \sin^{-1} \left(\sin \alpha \sqrt{\frac{B_{eq}}{B}} \right) \quad (1)$$

where B is the local magnetic field strength and B_{eq} is the equatorial magnetic field strength. We use the JRM33 (order 13) internal magnetic field model (Connerney et al., 2022) together with the CON2020 current sheet model (Connerney et al., 2020) to find B_{eq} by tracing the field line from *Juno*'s location to the magnetic equator using the JupiterMag community code (Wilson et al., 2023). The maximum observable equatorial pitch angle is limited by the ratio of the equatorial to the locally measured magnetic field (at $\alpha = 90^\circ$), $\alpha_{max} = \sin^{-1} \left(\sqrt{B_{eq}/B} \right)$. While analyzing the data, we consider only those particles that reach *Juno* from the magnetic equator, that is, particles with a local pitch angle $\alpha \in [0^\circ, 90^\circ]$ when it is in the southern hemisphere and $\alpha \in [90^\circ, 180^\circ]$ when it is in the northern hemisphere. The half-sky population reaching *Juno* from Jupiter is ignored as we are interested in the trapped distribution that may undergo charge exchange with the neutral tori.

We describe the conversion between count rate and phase space density (e.g., McComas et al., 2021) as well our methodology to create energy and pitch angle spectra, in Supporting Information S1. Example timeseries of pitch angle distributions are also shown in Figure S3 in Supporting Information S1.

3. Observations

3.1. Averaged Distribution and Variation With M-Shell

We constructed equatorial pitch angle distributions for all times during the prime mission when *Juno* was between M-shells of $M = 6$ and $M = 30$ and averaged the resulting distributions. These averages are shown in Figure 1 for the innermost M-shells. Missing or invalid data are excluded from the averaging process. Figure 1a shows the average distribution without normalization whereas Figures 1b–1d show the distributions averaged and normalized to the maximum/minimum PSD in each M-shell bin. *Juno*'s dwell time in each M-shell bin and availability of data with >77% coverage in equatorial pitch angle $\pm 5 R_J$ from the magnetic equator is shown in Figure 1f. On average, ~ 2 – 9 hr of data with near-complete equatorial pitch-angle coverage were available in each bin between $M = 8$ and $M = 22$. In these limited intervals, proton pitch angle distributions did not show significant abrupt changes due to magnetospheric injections.

Protons at the lowest energies considered (<50 keV) have fluxes that maximize at 0° equatorial pitch-angle and gradually decrease with increasing pitch-angle (Figure 1a). The relative depletion, or the ratio of maximum to minimum PSD is largest for M-shells 9, 10, and 11 (mean f_{\perp}/f_{\parallel} ranges from 1/4 to 1/2), and this ratio decreases

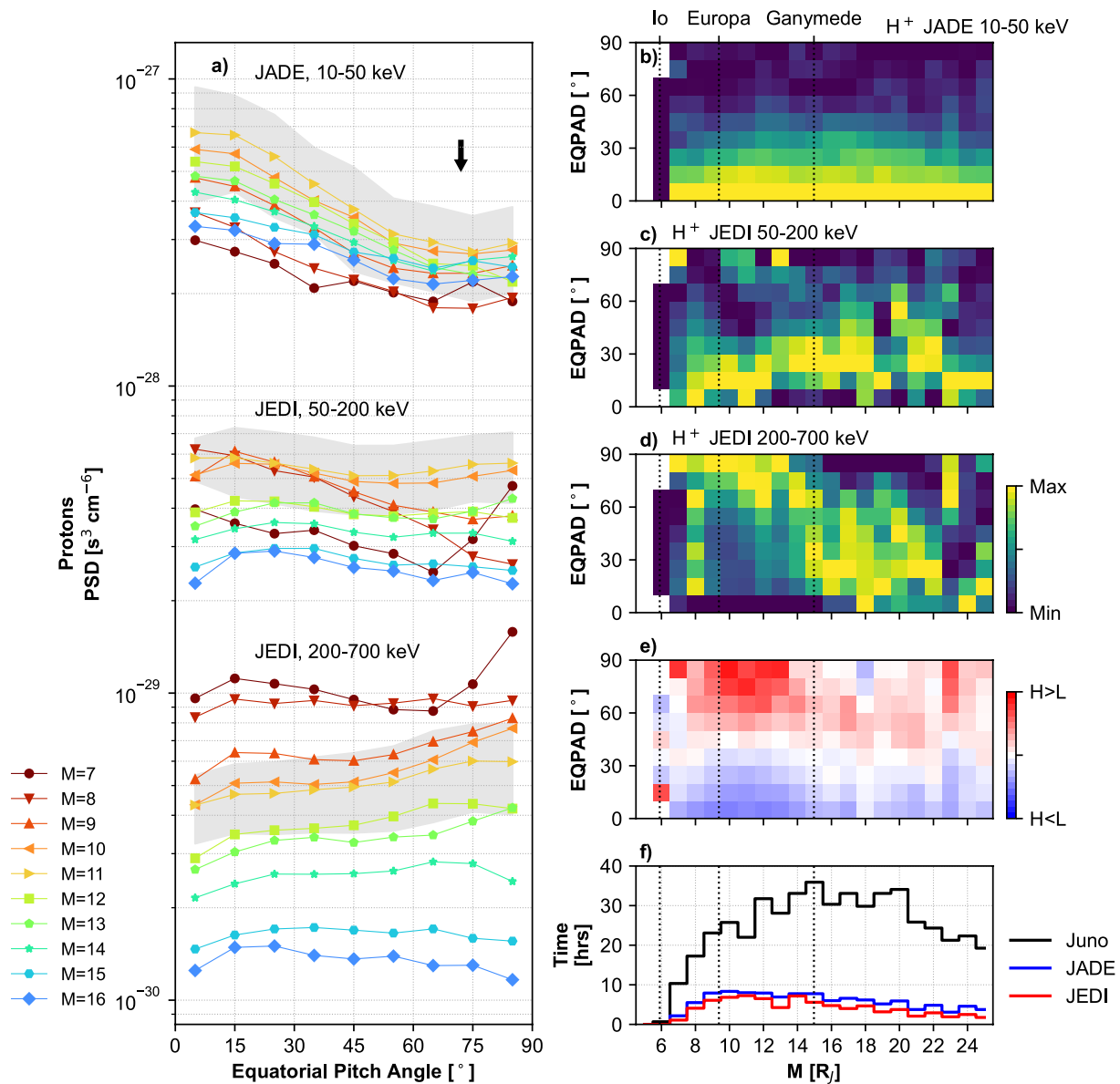


Figure 1. Mean H⁺ equatorial pitch-angle distributions at different M-shells for different energies. The gray region represents $\pm 1\sigma$ of all observations made within M-shell of $M = 11$ (b–d) Equatorial pitch-angle distributions normalized for each M-shell bin (e) Ratio of normalized spectra shown in (c) and (b). (f) Juno’s dwell time and data availability during the prime mission (2016–2021) in each M-shell bin and within $\pm 5 R_J$ of the magnetic equator in hours. Also shown is the total duration of valid data in each bin with $>77\%$ coverage in equatorial pitch angle.

with increasing M-shell. At higher energies (>200 keV), the proton distributions are either flat or increasing with equatorial pitch-angle (pancake-like), at all M-shells except for $M = 7$ and $M = 16$. At intermediate energies between 50 and 200 keV (Figure 1a), protons distributions vary at different M-shells. Inward of $M = 11$, one can see a depletion at 90° or 60° pitch-angle at $M = 10$ and $M = 11$. Pitch angle distributions of these protons are flatter beyond $M = 12$. The mean fluxes of 90° pitch angle protons are strongly depleted inward of Europa at $M = 8$ and $M = 9$ ($f_{\perp}/f_{\parallel} \approx 0.2$).

The variation of proton equatorial pitch-angle with M-shell can be seen clearly in Figures 1b–1d, where the distribution is normalized to each M-shell bin. At the lower energies, the highest fluxes are seen consistently at 0° pitch-angle (Figure 1b). At energies >200 keV, the highest fluxes inward of $M = 14$ are seen closer to 90° (Figure 1d). The 200–700 keV protons seem to transition from a pancake-like toward a more field-aligned distribution outward of $M = 16$ (Figure 1b). This trend was also observed by Shen et al. (2022) for 454–542 keV

and 0.98–2.01 MeV protons, who propose that this feature is consistent with particles gaining energy in the perpendicular direction due to conservation of the first adiabatic invariant (betatron acceleration) while being transported inward to regions of higher magnetic field (also similar to Clark et al. (2014) and Rymer et al. (2007) for electrons). Protons with energies between 10 and 50 keV do not follow this trend.

From 50 to 200 keV, the proton fluxes generally decrease with increasing pitch angle and minimize at $>60^\circ$ pitch-angle or more (Figure 1b). This depletion is not limited to M-shells near the Galilean moons and is seen for M-shells $M > 12$ as well. The proton “depletions” seen beyond $M = 12$ may be unrelated to charge exchange, as similar distributions are also seen for the lower (10–50 keV) and higher energies (>200 keV). Whereas inward of $M = 15$, the distribution for the lower and higher energy protons are different. This is more apparent in Figure 1e, which shows the ratio of the normalized spectra shown in panels d) and b). The differences are prominent inward of $M = 12$. If adiabatic acceleration due to radial transport produces the trend expected for the >200 keV population, then in the absence of other processes a similar distribution would be expected for protons at lower energies, which is not observed. Inward of $M = 12$, trapped protons at different energies have different pitch-angle distributions. Some possible reasons for this discrepancy are discussed in Section 3.3.

The normalized distributions exaggerate the anisotropy pitch angle distribution. This is the reason for the pixel-by-pixel variability seen in Figures 1c and 1d. Actual average distributions shown in Figure 1a are flat or weakly anisotropic for $M > 16$ at energies above 50 keV. In Supporting Information S1, we discuss the statistical significance of the observations and their variability.

3.2. Charge Exchange Interaction Rate

By using the differential flux measured by JADE and JEDI, we estimate interaction rates for different ion-neutral collisions. The rate of charge exchange is determined by the expression $(1/f)\partial f/\partial t = -\langle n \rangle \sigma v$, where $\langle n \rangle$ is the bounce- and drift-averaged neutral density, σ is the collision cross-section, v is the velocity of the incident ion, and f is the PSD, depending on M-shell, energy, equatorial pitch angle (Kollmann et al., 2011, 2016). This rate describes the relative change in PSD per time. Since the neutral density is not known in our case, we calculate an interaction rate via a different method that is independent of the neutral density but considers the distribution of incoming ion flux (Equation 2). The interaction rate can be used in combination with a neutral density, assumed or derived from numerical models, to estimate a local ENA production rate at different energies, thereby providing insight into the interaction of neutrals with the magnetospheric plasma (Note that this is different from an integrated or bounce-averaged ENA production rate).

$$r(E) = \sigma(E) \Delta E \int_{\Omega} j(E, \alpha) d\Omega \quad (2)$$

here $r(E)$ is the interaction rate in units of $[s^{-1}]$ at energy $E \pm \Delta E/2$, $\sigma(E)$ is the collision cross-section, ΔE is the width of the energy band, α is the pitch angle, j is the differential number flux in units of $[s^{-1} \text{ cm}^{-2} \text{ sr}^{-1} \text{ keV}^{-1}]$, and $d\Omega$ is the solid angle for a given pitch angle range. This rate represents the likelihood of a stationary neutral encountering an incident ion of certain energy in unit time, given an incident ion flux. The total charge exchange rate would be the sum of $r(E)$ over all energies, that is, $R = \sum r(E)$, which will have units of $[s^{-1}]$. These charge exchange rates are shown in Figure 2 for different intervals considering the $\text{H}^+\text{-O}$ and $\text{H}^+\text{-H}_2$ reactions, as O and H_2 are the most abundant neutral species in the inner magnetosphere. These rates are integrated over the unit sphere and hence are omnidirectional. Some periods exhibit a disconnect between the rates observed by JADE-I and JEDI 90/270, which could be due to the different fields-of-view for these instruments in equatorial pitch angle during one *Juno* spin.

Figure 2 shows that for all intervals, the interaction rate for a $\text{H}^+\text{-O}$ reaction is larger than that for $\text{H}^+\text{-H}_2$ above ~ 25 keV. This is because the collision cross-section of these two reactions crosses over at this energy (Lindsay & Stebbings, 2005; Tatsuo Tabata & Shirai, 2000), with that of the $\text{H}^+\text{-H}_2$ reaction falling off more sharply beyond 50 keV. Although there is no local maximum in the cross-sections, a peak can be seen in the interaction rate between 10 and 50 keV in panels a, c, d-f. This is due to the energy distribution of the proton fluxes, which peak at a similar energy. The interaction rates shown here can be used to predict the distribution of energetic neutral atoms (ENAs) that are created due to the charge exchange process. As previously described, the interaction rate shown here is independent of neutral density, where the product of this interaction rate with neutral density would yield the volume production rate of energetic neutrals.

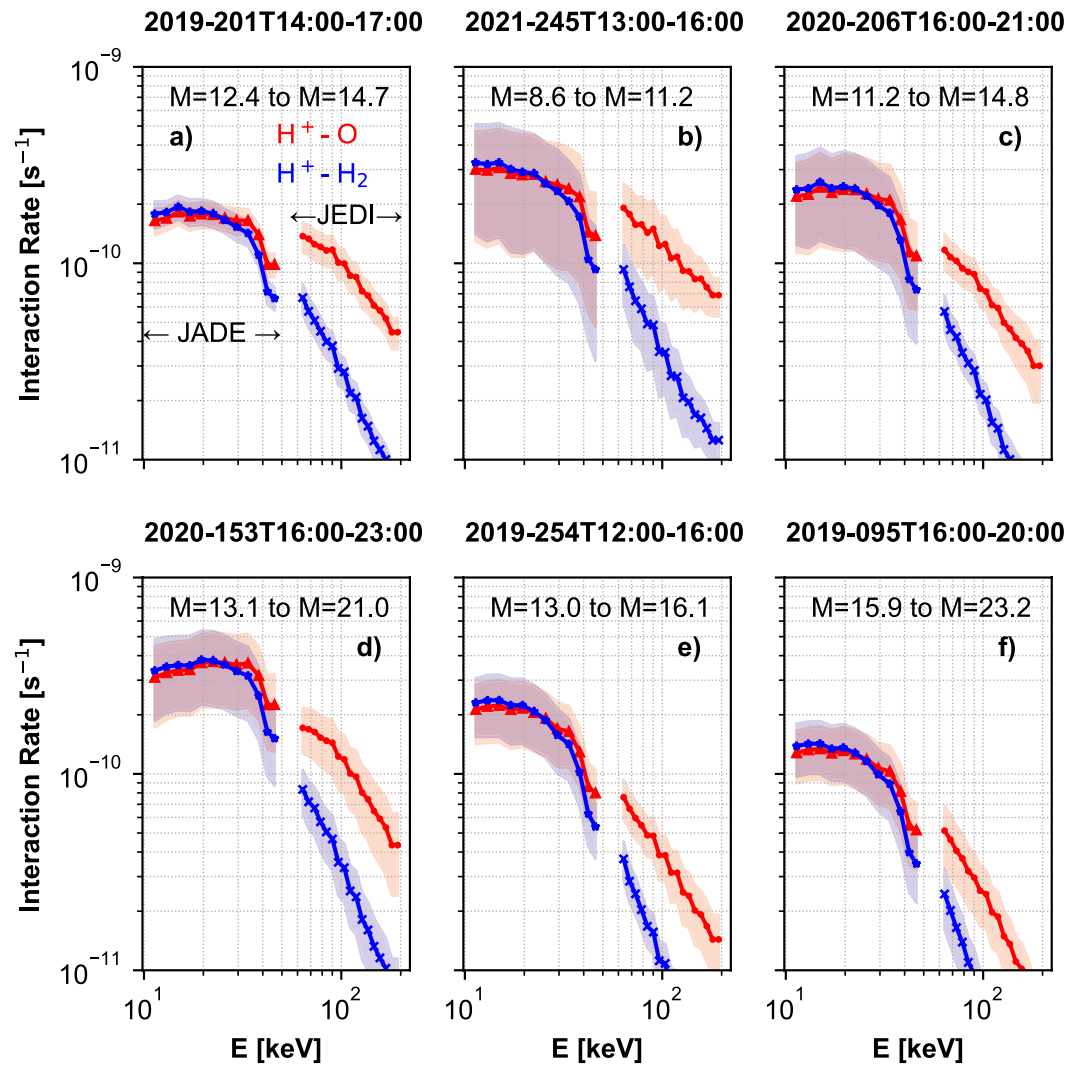


Figure 2. Estimated proton-neutral charge exchange interaction rates calculated from the observed proton fluxes and different collision cross-sections for different intervals. Solid lines are averages over the whole interval and error range represents 1σ of the observed rates.

The rate for each energy bin falls between $\sim 10^{-11}$ and $5 \times 10^{-9} \text{ s}^{-1}$. Summing over all energies between 10 and 200 keV, we calculate the total interaction rate for H-O to be in the range $1.9\text{--}6.3 \times 10^{-9} \text{ s}^{-1}$ and for H⁺-H₂ in the range from $1.6\text{--}4.8 \times 10^{-9} \text{ s}^{-1}$. As this is only between 10 and 200 keV energies, these numbers represent a lower limit on the rates. Smith et al. (2019) used the plasma densities observed by the *Galileo* spacecraft and estimate H⁺-O rates between 0.7 and $2.9 \times 10^{-7} \text{ s}^{-1}$ and H⁺-H₂ rates between 0.8 and $2.7 \times 10^{-7} \text{ s}^{-1}$ for different plasma conditions, which are about two orders of magnitude larger than those calculated in the present work. However, the ion-neutral charge exchange rates calculated by Smith et al. (2019) are calculated after assuming a neutral density, and particular ion velocity and cross-sections, and thus represent a different quantity from the rate described by Equation 2. In addition to the variability in the proton flux (shown in Figure 2), the error in the cross-sections for each reaction are also additional sources of uncertainty (not shown).

3.3. Interpretation of Pitch Angle Distributions

We summarize the various processes involved in the proton pitch angle distributions in Figure 3. Figures 1b–1d shows that protons at all energies tend to lower, field-aligned pitch angles at M-shells larger than $M \sim 16$. The 10–50 keV protons peak at 0° whereas for the 50–200 keV protons, the peak fluxes were seen at $\sim 30^\circ$ pitch angle. The predominantly field-aligned angle distributions seen at all energies could result from outward transport (e.g.,

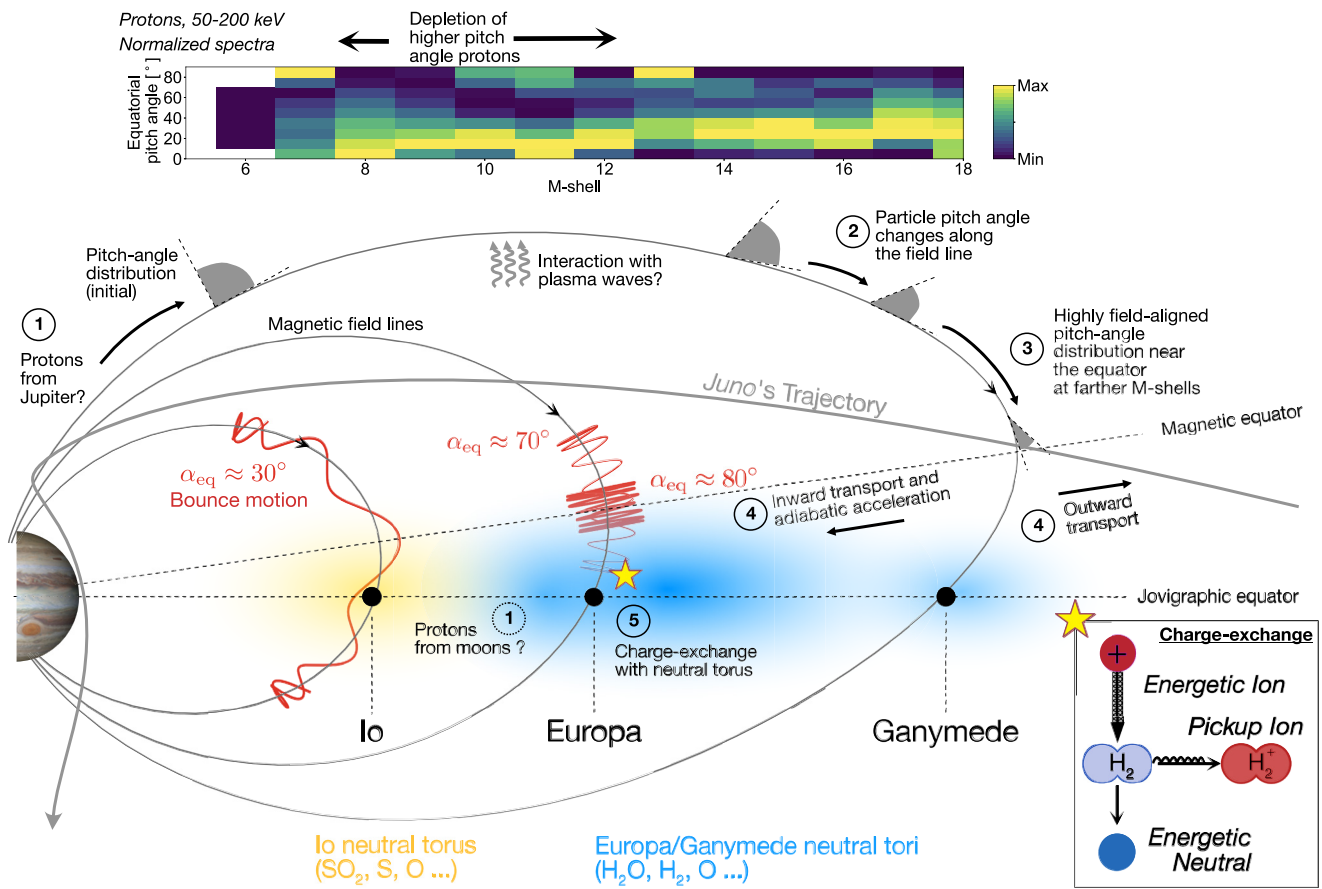


Figure 3. Schematic of Jupiter's inner magnetosphere highlighting possible proton transport processes and their influence on pitch angles. The inset shows a schematic of a charge exchange collision between an ion and an H₂ neutral molecule. The field lines represent a snapshot in time. In reality, the magnetic equator oscillates about the Jovigraphic equator due to the non-axisymmetric internal magnetic field of Jupiter.

due to interchange) and adiabatic deceleration in the perpendicular direction, similar to that observed for electrons by Rymer et al. (2008). However, if the 200–700 keV distribution at $M > 20$ represents an outward moving population, then it raises the question of how protons at these energies are produced inward of $M = 15$. Rather, Shen et al. (2022) and Kollmann et al. (2017) have observed a gradual increase of MeV proton flux with decreasing M-shell together with a positive slope of PSD versus M-shell inward of $M = 30$, that suggests weak inward diffusion. Hence, it is more likely that the 200–700 keV protons are moving inward and in the process transition from being “field-aligned” at $M > 20$ to pancake-like inward of $M \sim 16$. Similar transitions were noted by Tomás et al. (2004) and Shen et al. (2022) in the normalized proton and electron distributions, but it is unclear why this transition happens in the narrow range of M-shells between $M = 7$ and $M = 16$.

If inward adiabatic transport is expected to affect protons at all energies, why do pitch angle distributions for 10–50 keV and 50–200 keV protons differ from those of 200–700 keV protons inward of $M = 16$? One possible reason is that the lower energy protons at more equatorial pitch angles are being lost due to charge-exchange with neutral tori or cold ions. Then based on the differences in the pitch angle spectra (Figure 1e), charge exchange is occurring over a wide M-shell range between $M = 7$ and $M = 12$, which is consistent with the broad neutral tori seen in the model of Smith et al. (2019) and predicted from ENA observations by Mauk et al. (2003). Kollmann et al. (2016) used a charge exchange model to show that it is possible to reproduce the *Galileo* proton observations from a pancake-like pitch angle distribution as the source ($\propto \sin^{1.6} \alpha_{eq}$) using H₂ densities of $\sim 1.5\text{--}410 \text{ cm}^{-3}$. Moreover, the charge exchange rates shown in Figure 2 peak at energies between 10 and 100 keV. Charge exchange between keV energy protons and ions (Oⁿ⁺, Sⁿ⁺) is also possible though these reactions have cross-sections that are roughly an order of magnitude smaller than proton-neutral reactions, and heavy ion densities near Europa are expected to be between 1 and 50 cm⁻³, similar to the dominant neutral species (Smith et al., 2019). Also, other

neutral species like O, SO₂, H, H₂O (etc.) are also present but with lower densities, that could mean they are less important for charge exchange (Smith et al., 2019).

The observations inward of $M = 16$ could also result from protons coming directly from Jupiter's ionosphere at these M-shells. Jupiter-origin protons will have extremely small pitch angles at the magnetic equator due to the conservation of their first adiabatic invariant during their bounce motion (equatorial loss cone at $10 R_J$ is $\sim 0.02^\circ$). The preferentially field-aligned population observed at all energies at M-shells $M > 20$ is also consistent with outflow from Jupiter (shown in gray in Figure 3). Up-welling proton conics at energies ranging from 10 eV to 10 keV have been observed close to Jupiter's main auroral emission (Szalay et al., 2021) and the Io flux tube (Clark et al., 2020), which occupy M-shells between $M = 6$ and $M > 30$.

Lastly, proton pitch angle distributions may also be altered by pitch angle scattering due to resonant interaction with Alfvén or EMIC waves (Clark et al., 2023). At high latitudes and close to Jupiter, JEDI is able to resolve the atmospheric loss cone and has shown that >50 keV protons are scattered at the strong diffusion limit (flux inside the loss cone is equal to flux just outside it) in a large region around $M \sim 15$ – 18 (Mauk et al., 2022). While this finding suggests that pitch angle scattering of >50 keV protons may be strong, we find that the equatorial pitch angle distribution of >50 keV protons are not isotropic, which means that whatever process scatters protons in the atmospheric loss cone does not act on all equatorial pitch angle populations, or not fast enough compared to other mechanisms.

4. Conclusions

We examined the equatorial pitch angle distributions of energetic protons in the inner Jovian magnetosphere near the orbits of Io, Europa and Ganymede as measured by the JADE and JEDI instruments onboard the *Juno* spacecraft.

1. 10–50 keV protons have maximum fluxes in the field-aligned direction (0° equatorial pitch angle) at all M-shells between $M = 7$ to $M = 20$.
2. 200–700 keV protons transition from being predominantly field-aligned at $M > 16$ to pancake-like at $M = 7$ – 10 . Similar transitions have been observed previously for protons and electrons (Shen et al., 2022; Tomás et al., 2004) at Jupiter and electrons at Saturn (Clark et al., 2014), suggesting a universal process.
3. The abundance of field-aligned protons at all energies at $M > 16$ suggests that they could come from Jupiter's ionosphere and become field-aligned through adiabatic bounce motion.
4. The energy-dependent pitch angle distributions inward of $M = 16$ could result from charge exchange with neutral tori or from adiabatic inward transport of protons originating from the ionosphere. If charge exchange is responsible, the observations are consistent with a broad neutral torus present between $M = 7$ and $M = 12$.
5. Based on the observed particle fluxes and the collision cross-sections for H⁺-O and H⁺-H₂ reactions, we estimate a neutral-density-independent charge exchange interaction rate as a function of proton energy. The rates for both reactions maximize at energies of about ~ 10 – 50 keV.

There remain several open questions regarding proton transport at Jupiter. Future work could investigate how proton pitch angle distributions change with latitude to understand the proton source from Jupiter. Fokker-Plank modeling could also help understand the complex interaction between protons, adiabatic transport, plasma waves, and charge exchange with neutral tori. The neutral tori of Europa, and possibly Ganymede, remain poorly constrained. *Juno* has collected more data in this region during its extended mission, which could also be analyzed in the future.

Data Availability Statement

All data analyzed in this work is publicly available from the NASA Planetary Data System Plasma Interactions Node. In particular, we use data from the JADE, JEDI and magnetometer instruments, which is available at the following URLs—<https://doi.org/10.17189/1519715>, <https://doi.org/10.17189/1519713>, <https://doi.org/10.17189/1519711>. The JupiterMag community code can be accessed at <https://github.com/mattkjames7/JupiterMag>.

Acknowledgments

We acknowledge the work of the *Juno* mission team which led to the observations discussed in this work. This work was supported by NASA NFDAP Grant 80NSSC21K082. Q. Nénon acknowledges the support of CNES to the *Juno* mission. We thank the creators of the JupiterMag community code for making a useful tool for magnetic field line mapping.

References

Bagenal, F., & Dols, V. (2020). The space environment of Io and Europa. *Journal of Geophysical Research: Space Physics*, *125*(5), e2019JA027485. <https://doi.org/10.1029/2019JA027485>

Bagenal, F., Wilson, R. J., Siler, S., Paterson, W. R., & Kurth, W. S. (2016). Survey of Galileo plasma observations in Jupiter's plasma sheet: Galileo plasma observations. *Journal of Geophysical Research: Planets*, *121*(5), 871–894. <https://doi.org/10.1002/2016JE005009>

Bodisch, K. M., Dougherty, L. P., & Bagenal, F. (2017). Survey of voyager plasma science ions at Jupiter: 3. Protons and minor ions: Voyager minor ions. *Journal of Geophysical Research: Space Physics*, *122*(8), 8277–8294. <https://doi.org/10.1002/2017JA024148>

Bridge, H. S., Belcher, J. W., Lazarus, A. J., Sullivan, J. D., McNutt, R. L., Bagenal, F., et al. (1979). Plasma observations near Jupiter: Initial results from voyager 1. *Science (New York, N.Y.)*, *204*(4396), 987–991. <https://doi.org/10.1126/science.204.4396.987>

Clark, G., Mauk, B. H., Kollmann, P., Szalay, J. R., Sulaiman, A. H., Gershman, D. J., et al. (2020). Energetic proton acceleration associated with Io's footprint tail. *Geophysical Research Letters*, *47*(24), e2020GL090839. <https://doi.org/10.1029/2020GL090839>

Clark, G., Mauk, B. H., Paranicas, C., Kollmann, P., & Smith, H. T. (2016). Charge states of energetic oxygen and sulfur ions in Jupiter's magnetosphere. *Journal of Geophysical Research: Space Physics*, *121*(3), 2264–2273. <https://doi.org/10.1002/2015JA022257>

Clark, G., Paranicas, C., Santos-Costa, D., Livi, S., Krupp, N., Mitchell, D. G., et al. (2014). Evolution of electron pitch angle distributions across Saturn's middle magnetospheric region from MIMI/LEMMS. *Planetary and Space Science*, *104*, 18–28. <https://doi.org/10.1016/j.pss.2014.07.004>

Clark, G., Szalay, J. R., Sulaiman, A. H., Saur, J., Kollmann, P., Mauk, B. H., et al. (2023). Energetic proton acceleration by EMIC waves in Io's footprint tail. *Frontiers in Astronomy and Space Sciences*, *10*, 1016345. <https://doi.org/10.3389/fspas.2023.1016345>

Connerney, J. E. P., Benn, M., Bjarno, J. B., Denver, T., Espley, J., Jorgensen, J. L., et al. (2017). The Juno magnetic field investigation. *Space Science Reviews*, *213*(1–4), 39–138. <https://doi.org/10.1007/s11214-017-0334-z>

Connerney, J. E. P., Timmins, S., Herceg, M., & Joergensen, J. L. (2020). A Jovian magnetodisc model for the Juno era. *Journal of Geophysical Research: Space Physics*, *125*(10), e2020JA028138. <https://doi.org/10.1029/2020JA028138>

Connerney, J. E. P., Timmins, S., Oliverson, R. J., Espley, J. R., Joergensen, J. L., Kotsiaros, S., et al. (2022). A new model of Jupiter's magnetic field at the completion of Juno's prime mission. *Journal of Geophysical Research: Planets*, *127*(2), e2021JE007055. <https://doi.org/10.1029/2021JE007055>

Dougherty, L. P., Bodisch, K. M., & Bagenal, F. (2017). Survey of voyager plasma science ions at Jupiter: 2. Heavy ions. *Journal of Geophysical Research: Space Physics*, *122*(8), 8257–8276. <https://doi.org/10.1002/2017JA024053>

Frank, L. A., & Paterson, W. R. (2002). Galileo observations of electron beams and thermal ions in Jupiter's magnetosphere and their relationship to the auroras: Galileo observations of electron beams. *Journal of Geophysical Research*, *107*(A12), SMP35-1–SMP35-17. <https://doi.org/10.1029/2001JA009150>

Frank, L. A., Paterson, W. R., Ackerson, K. L., Vasyliunas, V. M., Coroniti, F. V., & Bolton, S. J. (1996). Plasma observations at Io with the Galileo spacecraft. *Science*, *274*(5286), 394–395. <https://doi.org/10.1126/science.274.5286.394>

Hamilton, D. C., Gloeckler, G., Krimigis, S. M., Bostrom, C. O., Armstrong, T. P., Axford, W. I., et al. (1980). Detection of energetic hydrogen molecules in Jupiter's magnetosphere by Voyager 2: Evidence for an ionospheric plasma source. *Geophysical Research Letters*, *7*(10), 813–816. <https://doi.org/10.1029/GL007i010p00813>

Hansen, C., Shemansky, D., & Hendrix, A. (2005). Cassini UVIS observations of Europa's oxygen atmosphere and torus. *Icarus*, *176*(2), 305–315. <https://doi.org/10.1016/j.icarus.2005.02.007>

Ip, W.-H. (1981). On the charge exchange loss of energetic charged particles in the Jovian magnetosphere. *Journal of Geophysical Research*, *86*(A13), 11246. <https://doi.org/10.1029/JA086iA13p11246>

Kim, T. K., Ebert, R. W., Valek, P. W., Allegrini, F., McComas, D. J., Bagenal, F., et al. (2020). Survey of ion properties in Jupiter's plasma sheet: Juno JADE-I observations. *Journal of Geophysical Research: Space Physics*, *125*(4), e2019JA027696. <https://doi.org/10.1029/2019JA027696>

Kollmann, P., Paranicas, C., Clark, G., Mauk, B. H., Haggerty, D. K., Rymer, A. M., et al. (2017). A heavy ion and proton radiation belt inside of Jupiter's rings: JUPITER'S innermost belt. *Geophysical Research Letters*, *44*(11), 5259–5268. <https://doi.org/10.1002/2017GL073730>

Kollmann, P., Paranicas, C., Clark, G., Roussos, E., Lagg, A., & Krupp, N. (2016). The vertical thickness of Jupiter's Europa gas torus from charged particle measurements: Europa gas torus. *Geophysical Research Letters*, *43*(18), 9425–9433. <https://doi.org/10.1002/2016GL070326>

Kollmann, P., Roussos, E., Paranicas, C., Krupp, N., Jackman, C. M., Kirsch, E., & Glassmeier, K.-H. (2011). Energetic particle phase space densities at Saturn: Cassini observations and interpretations: Energetic particles at Saturn. *Journal of Geophysical Research*, *116*(A5), A05222. <https://doi.org/10.1029/2010JA016221>

Kollmann, P., Roussos, E., Paranicas, C., Woodfield, E. E., Mauk, B. H., Clark, G., et al. (2018). Electron acceleration to MeV energies at Jupiter and Saturn. *Journal of Geophysical Research: Space Physics*, *123*(11), 9110–9129. <https://doi.org/10.1029/2018JA025665>

Lagg, A., Krupp, N., Woch, J., Livi, S., Wilken, B., & Williams, D. J. (1998). Determination of the neutral number density in the Io torus from Galileo-EPD measurements. *Geophysical Research Letters*, *25*(21), 4039–4042. <https://doi.org/10.1029/1998GL900070>

Lagg, A., Krupp, N., Woch, J., & Williams, D. J. (2003). In-situ observations of a neutral gas torus at Europa. *Geophysical Research Letters*, *30*(11), 1556. <https://doi.org/10.1029/2003GL017214>

Lindsay, B. G., & Stebbings, R. F. (2005). Charge transfer cross sections for energetic neutral atom data analysis. *Journal of Geophysical Research*, *110*(A12), A12213. <https://doi.org/10.1029/2005JA011298>

Mauk, B. H., Allegrini, F., Bagenal, F., Bolton, S. J., Clark, G., Connerney, J. E. P., et al. (2022). Loss of energetic ions comprising the ring current populations of Jupiter's middle and inner magnetosphere. *Journal of Geophysical Research: Space Physics*, *127*(5), e2022JA030293. <https://doi.org/10.1029/2022JA030293>

Mauk, B. H., Haggerty, D. K., Jaskulek, S. E., Schlemm, C. E., Brown, L. E., Cooper, S. A., et al. (2017). The Jupiter energetic particle detector instrument (JEDI) investigation for the Juno mission. *Space Science Reviews*, *213*(1–4), 289–346. <https://doi.org/10.1007/s11214-013-0025-3>

Mauk, B. H., Haggerty, D. K., Paranicas, C., Clark, G., Kollmann, P., Rymer, A. M., et al. (2017). Juno observations of energetic charged particles over Jupiter's polar regions: Analysis of monodirectional and bidirectional electron beams. *Geophysical Research Letters*, *44*(10), 4410–4418. <https://doi.org/10.1002/2016GL072286>

Mauk, B. H., Mitchell, D. G., Krimigis, S. M., Roelof, E. C., & Paranicas, C. P. (2003). Energetic neutral atoms from a trans-Europa gas torus at Jupiter. *Nature*, *421*(6926), 920–922. <https://doi.org/10.1038/nature01431>

Mauk, B. H., Mitchell, D. G., McEntire, R. W., Paranicas, C. P., Roelof, E. C., Williams, D. J., et al. (2004). Energetic ion characteristics and neutral gas interactions in Jupiter's magnetosphere. *Journal of Geophysical Research*, *109*(A9), A09S12. <https://doi.org/10.1029/2003JA010270>

Mauk, B. H., Szalay, J. R., Allegrini, F., Bagenal, F., Bolton, S. J., Clark, G., et al. (2023). How Bi-modal are Jupiter's main aurora zones? *Journal of Geophysical Research: Space Physics*, *128*(4), e2022JA031237. <https://doi.org/10.1029/2022JA031237>

- McComas, D. J., Alexander, N., Allegrini, F., Bagenal, F., Beebe, C., Clark, G., et al. (2017). The Jovian auroral distributions experiment (JADE) on the Juno mission to Jupiter. *Space Science Reviews*, 213(1–4), 547–643. <https://doi.org/10.1007/s11214-013-9990-9>
- McComas, D. J., Swaczyna, P., Szalay, J. R., Zirnstein, E. J., Rankin, J. S., Elliott, H. A., et al. (2021). Interstellar pickup ion observations halfway to the termination shock. *The Astrophysical Journal - Supplement Series*, 254(1), 19. <https://doi.org/10.3847/1538-4365/abee76>
- Nénon, Q., & André, N. (2019). Evidence of Europa neutral gas Torii from energetic sulfur ion measurements. *Geophysical Research Letters*, 46(7), 3599–3606. <https://doi.org/10.1029/2019GL082200>
- Rymer, A. M., Mauk, B. H., Hill, T. W., Paranicas, C., André, N., Sittler, E. C., et al. (2007). Electron sources in Saturn's magnetosphere: Electron sources at Saturn. *Journal of Geophysical Research*, 112(A2), A02201. <https://doi.org/10.1029/2006JA012017>
- Rymer, A. M., Mauk, B. H., Hill, T. W., Paranicas, C., Mitchell, D. G., Coates, A. J., & Young, D. T. (2008). Electron circulation in Saturn's magnetosphere: Electron circulation at Saturn. *Journal of Geophysical Research*, 113(A1), 10202. <https://doi.org/10.1029/2007JA012589>
- Shemansky, D. E., Yung, Y. L., Liu, X., Yoshii, J., Hansen, C. J., Hendrix, A. R., & Esposito, L. W. (2014). A new understanding of the Europa atmosphere and limits on geophysical activity. *The Astrophysical Journal*, 797(2), 84. <https://doi.org/10.1088/0004-637X/797/2/84>
- Shen, X., Li, W., Ma, Q., Nishimura, Y., Daly, A., Kollmann, P., et al. (2022). Energetic proton distributions in the inner and middle magnetosphere of Jupiter using Juno observations. *Geophysical Research Letters*, 49(16), e2022GL099832. <https://doi.org/10.1029/2022GL099832>
- Smith, H. T., Mitchell, D. G., Johnson, R. E., Mauk, B. H., & Smith, J. E. (2019). Europa neutral torus confirmation and characterization based on observations and modeling. *The Astrophysical Journal*, 871(1), 69. <https://doi.org/10.3847/1538-4357/aaed38>
- Smyth, W. H., & Marconi, M. L. (2003). Nature of the iogenic plasma source in Jupiter's magnetosphere. *Icarus*, 166(1), 85–106. [https://doi.org/10.1016/S0019-1035\(03\)00176-3](https://doi.org/10.1016/S0019-1035(03)00176-3)
- Smyth, W. H., & Marconi, M. L. (2006). Europa's atmosphere, gas tori, and magnetospheric implications. *Icarus*, 181(2), 510–526. <https://doi.org/10.1016/j.icarus.2005.10.019>
- Szalay, J. R., Allegrini, F., Bagenal, F., Bolton, S. J., Clark, G., Connerney, J. E. P., et al. (2021). Proton outflow associated with Jupiter's auroral processes. *Geophysical Research Letters*, 48(1), e2020GL091627. <https://doi.org/10.1029/2020GL091627>
- Szalay, J. R., Bagenal, F., Allegrini, F., Bonfond, B., Clark, G., Connerney, J. E. P., et al. (2020). Proton acceleration by Io's Alfvénic interaction. *Journal of Geophysical Research: Space Physics*, 125(1), e2019JA027314. <https://doi.org/10.1029/2019JA027314>
- Szalay, J. R., Clark, G., Livadiotis, G., McComas, D. J., Mitchell, D. G., Rankin, J. S., et al. (2022). Closed fluxtubes and dispersive proton conics at Jupiter's polar cap. *Geophysical Research Letters*, 49(9), e2022GL098741. <https://doi.org/10.1029/2022GL098741>
- Szalay, J. R., Smith, H. T., Zirnstein, E. J., McComas, D. J., Begley, L. J., Bagenal, F., et al. (2022). Water-group pickup ions from Europa-genic neutrals orbiting Jupiter. *Geophysical Research Letters*, 49(9), e2022GL098111. <https://doi.org/10.1029/2022GL098111>
- Tabata, T., & Shirai, T. (2000). Analytic cross sections for collisions of H⁺, H₂⁺, H₃⁺, H, H₂, and H- with hydrogen molecules. *Atomic Data and Nuclear Data Tables*, 76(1), 1–25. <https://doi.org/10.1006/adnd.2000.0835>
- Tomás, A., Woch, J., Krupp, N., Lagg, A., Glassmeier, K.-H., Dougherty, M. K., & Hanlon, P. G. (2004). Changes of the energetic particles characteristics in the inner part of the Jovian magnetosphere: A topological study. *Planetary and Space Science*, 52(5–6), 491–498. <https://doi.org/10.1016/j.pss.2003.06.011>
- Wilson, R. J., Vogt, M. F., Provan, G., Kamran, A., James, M. K., Brennan, M., & Cowley, S. W. H. (2023). Internal and external Jovian magnetic fields: Community code to serve the magnetospheres of the outer planets community. *Space Science Reviews*, 219(1), 15. <https://doi.org/10.1007/s11214-023-00961-3>